Strain-controlled switch between ferromagnetism and antiferromagnetism in 1T-CrX_2 (X = Se, Te) monolayers

H. Y. Lv,[1] W. J. Lu,[1,*] D. F. Shao,[1] Y. Liu,[1] and Y. P. Sun[1,2,3,†]

[1]*Key Laboratory of Materials Physics, Institute of Solid State Physics, Chinese Academy of Sciences, Hefei 230031, People's Republic of China*

[2]*High Magnetic Field Laboratory, Chinese Academy of Sciences, Hefei 230031, People's Republic of China*

[3]*Collaborative Innovation Center of Advanced Microstructures, Nanjing University, Nanjing 210093, People's Republic of China*

(Received 19 October 2015; published 14 December 2015)

We report on the strain-induced switch between ferromagnetic (FM) and antiferromagnetic (AFM) orderings in 1T-CrX_2 (X = Se, Te) monolayers based on first-principles calculations. The $CrSe_2$ and $CrTe_2$ monolayers without strains are found to be AFM and FM, respectively. Under biaxial tensile strain, the $CrSe_2$ monolayer tends to be FM when the strain is larger than 2%. The FM state is further stabilized when the strain is increased. Moreover, the $CrSe_2$ monolayer becomes half metallic when the tensile strain is larger than 10%, while for the $CrTe_2$ monolayer, the critical strain at which the transition between the FM and AFM states occurs is compressive, of −1%. Relatively small tensile strains of 4% and 2%, respectively, can enhance the Curie temperature of the $CrSe_2$ and $CrTe_2$ monolayers above room temperature. The strain-induced switch between the FM and AFM states in a $CrSe_2$ ($CrTe_2$) monolayer can be understood by the competition between the AFM Cr-Cr direct exchange interaction and the FM Cr-Se(Te)-Cr superexchange interaction. Tunable and attractive magnetic and electronic properties controlled by flexible strain are desirable for future nanoelectronic applications.

DOI: 10.1103/PhysRevB.92.214419 PACS number(s): 73.22.−f, 75.50.Cc, 75.75.−c, 81.05.Zx

I. INTRODUCTION

Since the discovery of graphene, which is an atomic layer exfoliated from graphite, two-dimensional (2D) materials have attracted considerable research interest in recent years, due to their potential applications in nanoelectronics based on their diverse and attractive properties. Similar to graphite, most of the layered materials are stacked, with their building blocks connected by weak van der Waals interactions. Thus it is possible to obtain few layers or even a monolayer from their bulk counterparts [1–3]. Among various kinds of layered materials, transition metal dichalcogenides (TMDs) stand out because some of them exhibit many more exciting properties compared to the star material, graphene. For instance, a MoS_2 monolayer was found to be a semiconductor with a sizable direct band gap of about 1.8–1.9 eV [4–6], overcoming the disadvantage of a zero band gap in graphene when applied in field effect transistors (FETs) and optoelectronic devices.

With respect to spintronic applications, 2D ferromagnets with high Curie temperatures are desirable. However, neither graphene nor most of the TMD monolayers are intrinsically magnetic. Many methods can be used to induce magnetic orderings in TMD monolayers, mainly including doping [7–10], hydrogenation [11–14], and forming zigzag edges [15,16]. In nanoelectronic applications, however, we expect that the magnetism can be precisely and flexibly controlled. The methods mentioned above are somewhat rough as compared with practical requirements. Recently, VX_2 [17], NbX_2 [18], and MnX_2 [19] (X = S, Se) monolayers were theoretically predicted to exhibit ferromagnetic (FM) behavior, broadening the properties of pristine 2D monolayers.

Very recently, the metastable compound 1T-$CrTe_2$ was successfully synthesized in experiments and it exhibits a FM property with a high Curie temperature of 310 K [20], while it was reported that the $CrSe_2$ compound is antiferromagnetic (AFM) and its magnetic property can be tuned by substituting Cr with V or Ti [21]. Then, the question is, what is the origin of the different magnetic properties of $CrSe_2$ and $CrTe_2$ compounds? On the other hand, 2D materials are needed when applied in nanoelectronic devices. Since CrX_2 (X = Se, Te) compounds exhibit various and appealing magnetic behaviors, can they retain these properties when they are exfoliated into monolayers and can the magnetic properties be further tuned by an external method, such as strain [17,18]? These questions deserve a careful investigation.

In this paper, we investigate the electronic and magnetic properties of 1T-CrX_2 (X = Se, Te) monolayers by using first-principles calculations. The results show that, similar to their bulk counterparts, pristine $CrSe_2$ and $CrTe_2$ monolayers are AFM and FM, respectively. Interestingly, we find that the switch between FM and AFM can be realized in both of the monolayers by applying relatively small strains, and the Curie temperatures can be enhanced above room temperature. The magnetic and electronic properties of $CrSe_2$ and $CrTe_2$ monolayers can be easily tuned by an external strain, making them promising candidates in future spintronic applications.

II. COMPUTATIONAL DETAILS

The electronic and magnetic properties were investigated based on first-principles calculations within the framework of the density functional theory (DFT) [22], as implemented in the QUANTUM ESPRESSO code [23]. Ultrasoft pseudopotentials with scalar-relativistic modes were used to represent the interaction between electrons and ions. The exchange-correlation potential was in the form of the Perdew-Burke-Ernzerhof (PBE) expression [24] of the generalized-gradient

*Corresponding author: wjlu@issp.ac.cn

†Corresponding author: ypsun@issp.ac.cn

approximation (GGA). The cutoff energy was set to be 544 eV. For each monolayer, a vacuum region of 15 Å was added so that the interactions between the monolayer and its period image can be neglected. We used $2 \times 2 \times 1$ and $3 \times 3 \times 1$ supercells for the collinear [the spins are aligned in parallel or antiparallel directions; the spin configurations are shown in Figs. 2(a) and 2(b)] and noncollinear [the spin configuration is shown in Fig. 2(f)] magnetic calculations, respectively. For structural relaxations, the Brillouin zones were sampled with $8 \times 8 \times 1$ and $4 \times 4 \times 1$ Monkhorst-Pack k-point meshes for the above two supercells, respectively. For the electronic properties of the collinear calculations, a $10 \times 10 \times 1$ Monkhorst-Pack k-point mesh was used.

As both $CrSe_2$ and $CrTe_2$ compounds have metastable structures, the lattice parameters were kept fixed at the experimental values when doing the calculations for the bulk [20,21]. For the monolayers, when no strain is applied, the in-plane experimental lattice constants of the corresponding bulks were used. The value of the in-plane biaxial strain is defined as $\varepsilon = (a - a_0)/a_0 \times 100\%$, where a and a_0 are the in-plane lattice constants of the strained and unstrained monolayers, respectively. At a particular strain condition, the atomic positions were fully relaxed until the force acting on each atom was less than 2.6×10^{-4} eV/Å.

III. RESULTS AND DISCUSSION

A. $CrSe_2$ and $CrTe_2$ bulks

The $1T$-$CrSe_2$ and $CrTe_2$ compounds were found to have AFM and FM ground states, respectively [20,21]. They crystallize in the space group of $P\bar{3}m1$ (No. 164), with the layered structures stacked by Se-Cr-Se and Te-Cr-Te sandwich layers along the c axis, respectively, as shown in Fig. 1(a). Within the sandwich layer, the Cr atoms are octahedrally coordinated and covalently bonded by the six nearest-neighboring Se/Te atoms, forming a hexagonal layer sandwiched between the two layers of Se/Te atoms, while in between the layers, the interactions are mainly of the van der Waals type.

To reveal the origin of the different magnetic orderings in $CrSe_2$ and $CrTe_2$ compounds, we first calculate their Fermi surfaces (FSs) without spin polarizations, which are shown in Figs. 1(b) and 1(c), respectively. For the $CrSe_2$ bulk, the FS is composed of two holelike bellied cylinders, one centered along the Γ-A line and the other along the K-H line. The two bellied cylinders indicate that the FS may have a nesting feature, and the nesting vector is along the Γ-K direction. FS nesting may be the origin of the magnetic ground state, which will be discussed later. For the $CrTe_2$ bulk, however, one holelike bellied cylinder centered along the Γ-A line and one electronlike cylinder centered along the M-L line form the FS, in good agreement with the previous report [20]. In the a-b plane, the FS does not exhibit any nesting property.

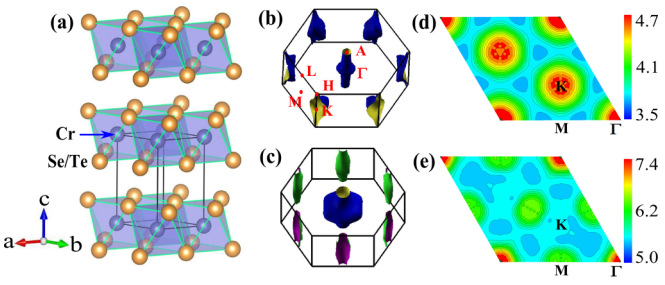

FIG. 1. (Color online) (a) Crystal structure of $CrSe_2/CrTe_2$ bulk; Fermi surface without spin polarization for (b) $CrSe_2$ and (c) $CrTe_2$ bulks; real part of the electron susceptibility χ' with $q_z = 0$ for (d) $CrSe_2$ and (e) $CrTe_2$ bulks.

The magnetic properties may be controlled by FS topology [25], which can be understood by the Fourier transformed exchange coupling constant expressed as [26–28]

$$J(\mathbf{q}) \propto \frac{1}{N}\sum_{\mathbf{k}} I(\mathbf{k},\mathbf{q})\frac{f(\varepsilon_{\mathbf{k}}) - f(\varepsilon_{\mathbf{k+q}})}{\varepsilon_{\mathbf{k}} - \varepsilon_{\mathbf{k+q}}} \approx I\chi'(\mathbf{q}), \qquad (1)$$

where

$$\chi'(\mathbf{q}) = \frac{1}{N}\sum_{\mathbf{k}} \frac{f(\varepsilon_{\mathbf{k}}) - f(\varepsilon_{\mathbf{k+q}})}{\varepsilon_{\mathbf{k}} - \varepsilon_{\mathbf{k+q}}}. \qquad (2)$$

Here, $\mathbf{q}$ represents the Fourier component of a generic perturbation, $I(\mathbf{k},\mathbf{q})$ is the exchange integral, which is approximated to a constant I in real cases, f is the Fermi-Dirac distribution function, $\varepsilon_{\mathbf{k}}$ is the eigenvalue of the electron $\mathbf{k}$, χ' refers to the real part of the electron susceptibility, and N is the total number of $\mathbf{k}$ points. The maximum of $J(\mathbf{q})$ and thus the maximum of χ' determine a periodic magnetic moment arrangement with a propagation vector $\mathbf{q}$. We can deduce from Eqs. (1) and (2) that when the propagation vector $\mathbf{q}$ coincides with the FS nesting vector, the maximum of χ' appears.

From Fig. 1(d) we can see that, for $CrSe_2$, the maximum value of χ' appears at $\mathbf{q} = \frac{1}{3}\mathbf{a}^* + \frac{1}{3}\mathbf{b}^*$, confirming the existence of FS nesting in the $CrSe_2$ bulk. The nesting vector $\mathbf{q}$ indicates that there exists a magnetic configuration with a $3 \times 3 \times 1$ supercell in real space, which may correspond to the AFM ground state measured in the experiment [21]. However, in the experiment, the details of the spin ordering are not reported. As discussed later, there exists a frustration in the spins of the Cr atoms in this system. A noncollinear AFM configuration with the spin vectors of the nearest-neighboring Cr atoms at 120° to each other [see Fig. 2(f)] form a $3 \times 3 \times 1$ supercell exactly, consistent with the nesting result, so it may be one possibility of the spin arrangement in this system, which needs to be further checked by the experiment. Actually, this triangle arrangement of the spin structure has been found in $LiCrS_2$ [29]. For the $CrTe_2$ compound, however, except for the maximum near the Γ point, we cannot see any other local maximum of χ' in the (q_x, q_y) plane [see Fig. 1(e)], which may be responsible for the uniform arrangement of the spins (FM configuration) observed in the experiment.

B. $CrSe_2$ and $CrTe_2$ monolayers

The interesting magnetic properties of the $CrSe_2$ and $CrTe_2$ bulks inspire us to explore how their monolayer counterparts will perform, which will have potential applications in nanoelectronics. First, we examine the ground states of the $CrSe_2$ and $CrTe_2$ monolayers. The two collinear FM and AFM magnetic configurations considered in this work are shown in Figs. 2(a) and 2(b), respectively. Figure 2(c) is the side view of the monolayer, with the Cr layer sandwiched between two Se

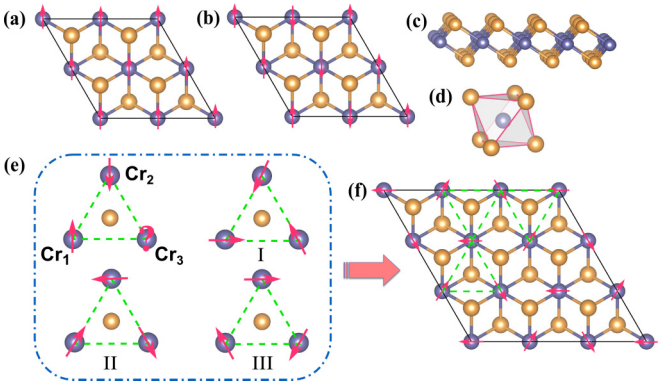

FIG. 2. (Color online) Top views of collinear (a) ferromagnetic and (b) antiferromagnetic configurations; (c) side view of the $CrSe_2/CrTe_2$ monolayer; (d) the octahedron formed by nearest Se/Te atoms surrounding the Cr atom; (e) (upper left) spin frustration arising from the triangular geometry of the nearest three Cr atoms when their magnetic moments are antiferromagnetically aligned with each other; (the rest) the three solutions of the spin frustrations, with the spin vectors of the three Cr atoms at 120° to each other, labeled as "I," "II," and "III," respectively; (f) noncollinear antiferromagnetic configuration of the $CrSe_2/CrTe_2$ monolayer constructed by the three solutions in (e). Blue and orange balls represent Cr and Se/Te atoms, respectively.

or Te layers. Each Cr atom is in the center of the octahedron formed by the nearest Se/Te atoms, as shown in Fig. 2(d). The nearest Cr atoms form an equilateral triangle [see the upper left corner of Fig. 2(e)]. In the collinear AFM configuration, if we assume the spins of the Cr_1 and Cr_2 atoms are up and down, respectively, then the (up or down) spin of the Cr_3 atom will be the same as the spin of the Cr_1 or Cr_2 atom. That is to say, the spin of the Cr_3 atom cannot align simultaneously antiparallel to the spins of Cr_1 and Cr_2 atoms, so it is frustrated. The three solutions of this spin frustration are demonstrated in Fig. 2(e), labeled as "I," "II," and "III," respectively. The spin vectors of the three atoms are at 120° to each other. Combining these three cases, we construct a noncollinear AFM configuration with a $3 \times 3 \times 1$ supercell, as shown in Fig. 2(f).

The total energy calculations of the three different magnetic configurations [FM, AFM1 (collinear), and AFM2 (noncollinear)] show that the ground states of the $CrSe_2$ and $CrTe_2$ monolayers are AFM and FM, respectively, the same as the results of the corresponding bulk structures. For the $CrSe_2$ monolayer, the energy of the noncollinear AFM configuration is relatively lower than that of the collinear one, so the triangular AFM spin arrangement with a $3 \times 3 \times 1$ supercell is the ground state of the $CrSe_2$ monolayer, which is consistent with the result of FS nesting in the $CrSe_2$ bulk, as discussed above. The intrinsic magnetic ground states in the two monolayers are very useful and it is interesting to find ways to further tune the magnetic properties.

Strain is a flexible method to tune the properties of 2D layers. We then study the strain-dependent magnetic properties of $CrSe_2$ and $CrTe_2$ monolayers. In-plane tensile and compressive biaxial strains are applied. The relative total energies of the three different magnetic configurations as a function of the strain are shown in Fig. 3. The energies of the nonmagnetic (NM) systems are much larger than those of the

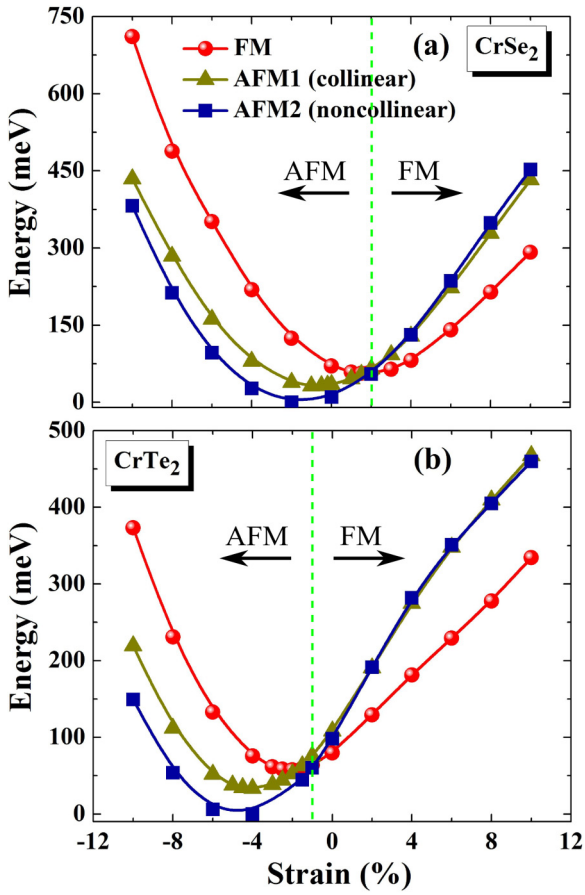

FIG. 3. (Color online) Relative total energies of three different magnetic configurations [FM, AFM1 (collinear), and AFM2 (noncollinear)] as a function of biaxial strain for (a) $CrSe_2$ and (b) $CrTe_2$ monolayers.

magnetic ones, so they are not displayed here. For the $CrSe_2$ monolayer [see Fig. 3(a)], the spin ordering tends to be FM when the tensile strain is larger than 2%. Moreover, the energy difference between the FM and AFM orderings becomes larger and larger with increasing tensile strain, so the applied tensile strain can stabilize the FM state in this system. On the other hand, the $CrSe_2$ monolayer remains AFM when the tensile strain is smaller than 2% or the applied strain is compressive. So, there exists a critical strain of 2% at which the transition between the FM and AFM states takes place. For the $CrTe_2$ monolayer, it remains in the FM state when tensile strain is applied. The same as in the case of the $CrSe_2$ monolayer, the energy difference between the FM and AFM states becomes larger and larger when the tensile strain is increased. The spin ordering becomes AFM when the absolute value of the compressive strain is larger than 1%, so the critical strain of the $CrTe_2$ monolayer is −1%. From the calculated total energies of the three different spin orderings as a function of the strain, we can see that the magnetic states of the $CrSe_2$ and $CrTe_2$ monolayers can be effectively tuned by external strains. Relatively small strains can induce the transitions between the AFM and FM states in the two kinds of materials.

As both $CrSe_2$ and $CrTe_2$ monolayers can exhibit FM properties, it is interesting to evaluate the Curie temperature

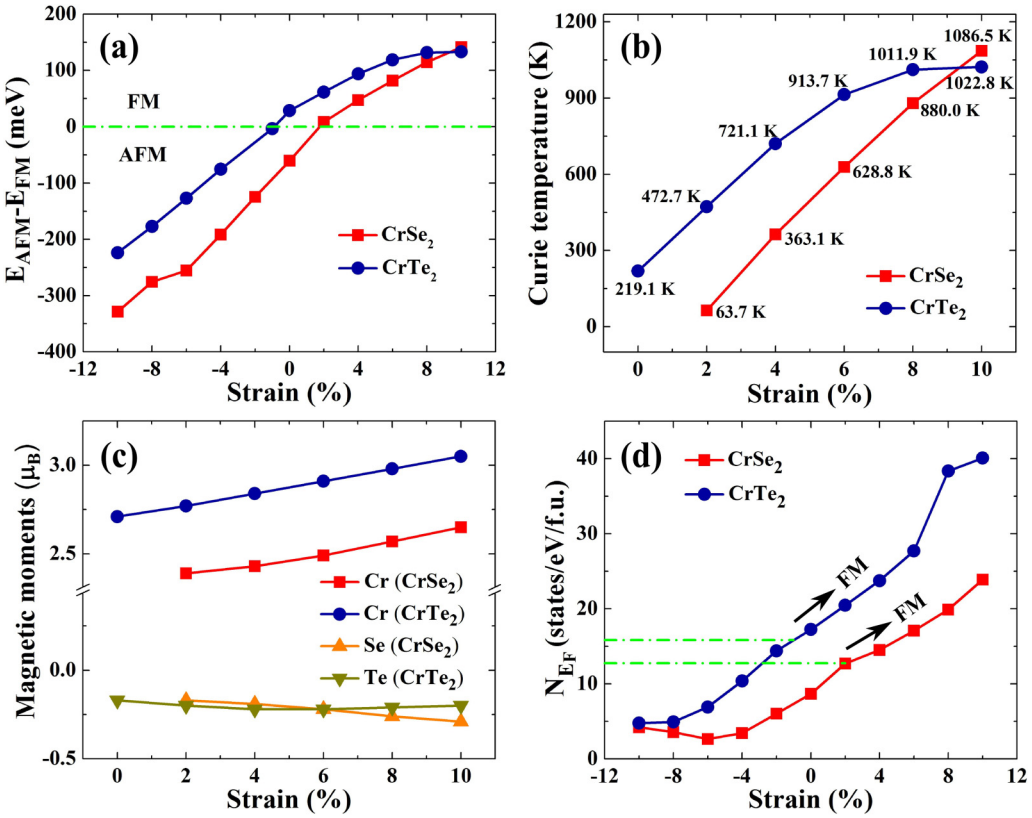

FIG. 4. (Color online) Strain dependence of (a) the energy difference ΔE ($=E_{\mathrm{AFM}} - E_{\mathrm{FM}}$) between AFM and FM states in one unit cell, (b) the Curie temperature T_C in FM states, (c) magnetic moments on Cr and Se/Te atoms in FM states, and (d) the number of density of states (DOS) at the Fermi energy N_{E_F} in the nonmagnetic (NM) states for $CrSe_2/CrTe_2$ monolayers.

T_C, which is an important design parameter for practical usage. The T_C of $CrSe_2/CrTe_2$ monolayers are estimated based on the mean-field theory and Heisenberg model [7,11,30], where T_C is expressed as $k_B T_C = (2/3)\Delta E$. Here, k_B is the Boltzmann constant and ΔE ($=E_{\mathrm{AFM}} - E_{\mathrm{FM}}$) is the energy difference between the AFM and FM states in one unit cell. The calculated ΔE and T_C of the $CrSe_2/CrTe_2$ monolayers under different biaxial strains are shown in Figs. 4(a) and 4(b), respectively. We can see that for both $CrSe_2$ and $CrTe_2$ monolayers, the ΔE in the FM states and therefore the T_C increase with increasing strain. For the $CrSe_2$ monolayer, the T_C is 63.7 K at a strain of 2%. When the strain reaches 4%, the T_C increases rapidly to 363.1 K, larger than room temperature. At the largest strain of 10%, a T_C as high as 1086.5 K can be obtained. For the $CrTe_2$ monolayer, as discussed above, it exhibits FM behavior when no strain is applied. The calculated energy difference ΔE is 28.5 meV and T_C is 219.1 K, which is smaller than that of the $CrTe_2$ bulk (310 K) [20]. However, when a small strain of 2% is applied, the T_C can be enhanced above room temperature, i.e., 472.7 K. At a strain of 10%, the T_C of the $CrTe_2$ monolayer can reach as high as 1022.8 K. The magnetic moments of Cr (μ_{Cr}) and Se/Te atoms ($\mu_{\mathrm{Se}}/\mu_{\mathrm{Te}}$) for $CrSe_2/CrTe_2$ monolayers are shown in Fig. 4(c). We can see that for both materials, μ_{Cr} are much larger than μ_{Se} or μ_{Te} and increase monotonically with an increase of applied strains.

In what follows, we will discuss the origin of the strain-induced magnetic evolution in $CrSe_2/CrTe_2$ monolayers. First, the transition between AFM and FM states can be roughly explained by the Stoner criterion which is expressed as

$$I N_{E_F} > 1, \tag{3}$$

where N_{E_F} is the number of the density of states (DOS) at the Fermi energy in the NM state. Figure 4(d) shows the calculated N_{E_F} as a function of the strain for $CrSe_2$ and $CrTe_2$ monolayers. It is clearly seen that the N_{E_F} generally increases with increasing strain. At the critical strain where the transition between the AFM and FM states occurs, the values of N_{E_F} are 12.7 and 15.8 for the $CrSe_2$ and $CrTe_2$ monolayers, respectively. When the strain is further increased, the N_{E_F} increases as well, so the FM state becomes more and more stable.

On the other hand, we notice that when the strain is increased, the distance between a Cr atom and its nearest-neighboring Cr atom (denoted as $d_{\mathrm{Cr\text{-}Cr}}$) increases dramatically with an increase of strain, as shown in Fig. 5(a). For the $CrSe_2$ ($CrTe_2$) monolayer, $d_{\mathrm{Cr\text{-}Cr}}$ changes from 3.40 Å (3.79 Å) without strain to 3.74 Å (4.17 Å) at a strain of 10%, both increasing by 10% when the strain is increased by 10%. However, the bond lengths between the Cr and Se (Te) atoms [denoted as $d_{\mathrm{Cr\text{-}Se}}$ ($d_{\mathrm{Cr\text{-}Te}}$)] increase slowly with increasing strain. For the $CrSe_2$ ($CrTe_2$) monolayer, $d_{\mathrm{Cr\text{-}Se}}$ ($d_{\mathrm{Cr\text{-}Te}}$) changes from 2.47 Å (2.70 Å) without strain to 2.54 Å (2.75 Å) at a strain of 10%, increasing only by 2.83% (1.85%) when the strain is increased by 10%. This property can be ascribed to the sandwiched structure of the $CrSe_2/CrTe_2$ monolayers. When the system is stretched in plane, $d_{\mathrm{Cr\text{-}Cr}}$

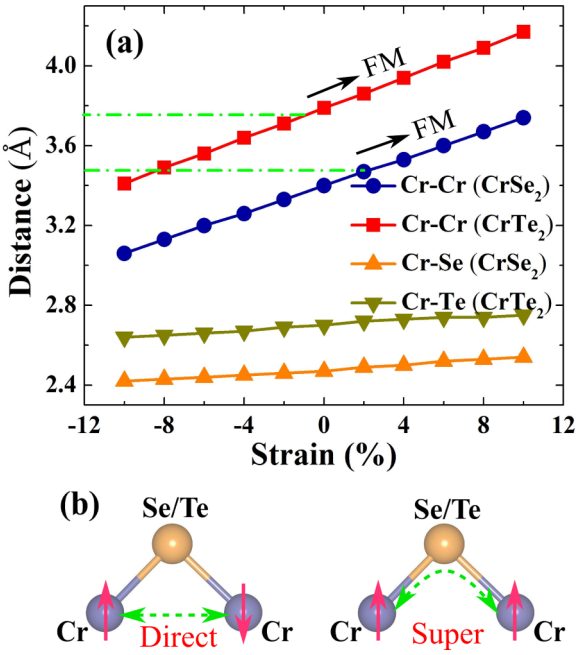

FIG. 5. (Color online) (a) Distance between the nearest-neighboring Cr atoms $d_{\text{Cr-Cr}}$ and bond length between the Cr and Se (Te) atoms $d_{\text{Cr-Se}}$ ($d_{\text{Cr-Te}}$) as a function of the applied biaxial strain for $CrSe_2$ and $CrTe_2$ monolayers. (b) Illustrations of the Cr-Cr direct exchange (left panel) and Cr-Se(Te)-Cr superexchange (right panel) interactions in $CrSe_2$/$CrTe_2$ monolayers.

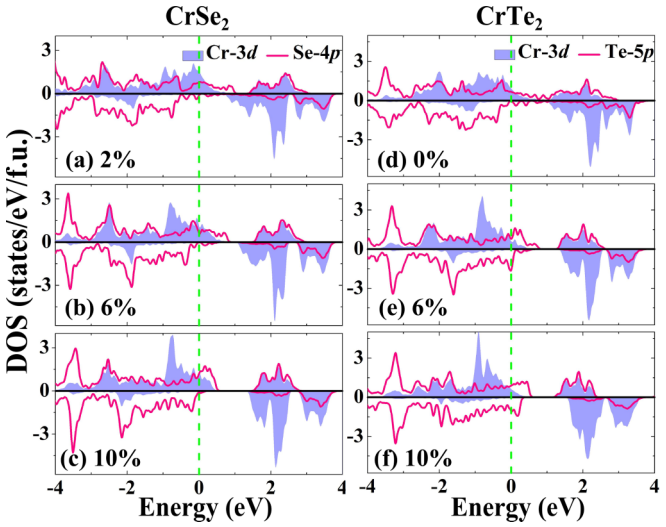

FIG. 6. (Color online) Partial density of states (PDOS) of Cr $3d$ and Se $4p$ orbitals for the $CrSe_2$ monolayer in the FM ground state at tensile strains of (a) 2%, (b) 6%, and (c) 10%; PDOS of Cr $3d$ and Te $5p$ orbitals for the $CrTe_2$ monolayer in the FM ground state at tensile strains of (d) 0%, (e) 6%, and (f) 10%. The positive and negative values represent the DOS of up and down spins, respectively. The Fermi level is set to be 0 eV.

increases accordingly since all the Cr atoms are in the same layer, while the outside Se/Te atom layers move closer to the Cr atom layer, keeping the $d_{\text{Cr-Se}}$ ($d_{\text{Cr-Te}}$) slightly changed. For graphene, since all the carbon atoms are in the same layer, the bond length increases monotonically by 10% when a tensile strain of 10% is applied. The relatively small changes in the bond lengths in $CrSe_2$/$CrTe_2$ monolayers indicate they can withstand relatively larger tensile strains before structural disruption and thus provide a possibility to well control the magnetic properties by a wide range of external strain.

Based upon the different behaviors of $d_{\text{Cr-Cr}}$ and $d_{\text{Cr-Se}}$ ($d_{\text{Cr-Te}}$) upon applied strain, the mechanism of the transition between FM and AFM states and the strain-tunable stability of the FM states can be understood by the competition between two different exchange interactions. First, since the $d_{\text{Cr-Cr}}$ is not very large, the direct exchange interaction between the two nearest-neighboring Cr atoms (denoted as J_D) cannot be neglected, which leads to the AFM arrangement of the two Cr atoms [see the left panel of Fig. 5(b)]. Second, as shown in the right panel of Fig. 5(b), the two nearest-neighboring Cr atoms are connected by a Se/Te atom, thus a superexchange interaction mediated by the middle Se/Te atom exists. Since the Cr-Se(Te)-Cr bond angle is close to 90° and the number of $3d$ electrons of the Cr atom is 5, according to the Goodenough-Kanamori-Anderson (GKA) rules [31–33], the Cr-Se(Te)-Cr superexchange interaction (denoted as J_S) will induce a FM arrangement of the two nearest-neighboring Cr atoms. Therefore, the magnetic states of $CrSe_2$/$CrTe_2$ monolayers are determined by $J_D + J_S$, where J_D and J_S are negative and positive, respectively. For a $CrSe_2$ monolayer without strain, $|J_D|$ is relatively larger than J_S, so $J_D + J_S < 0$ and the system exhibits AFM properties. When tensile strain is applied, as discussed above, the $d_{\text{Cr-Cr}}$ increases much faster than $d_{\text{Cr-Se}}$, so $|J_D|$ decreases much faster than J_S. At a critical strain of 2%, J_S is equal to $|J_D|$ and $J_D + J_S = 0$. When the strain is larger than 2%, J_S prevails in determining the magnetic property and $J_D + J_S > 0$, so the $CrSe_2$ monolayer becomes FM. Moreover, since $|J_D|$ decreases much faster than J_S with increasing strain, $J_D + J_S$ increases as a function of the strain when the strain is further increased. As a result, the energy difference between the FM and AFM states becomes larger and the FM state is stabilized by the applied tensile strain. The case for the $CrTe_2$ monolayer is very similar, except that the critical strain is compressive, of −1%. For the $CrTe_2$ monolayer without strain, the $|J_D|$ is relatively smaller than J_S, so $J_D + J_S > 0$ and the system is FM. From the above discussion, we can see that the $d_{\text{Cr-Cr}}$ plays an important role in determining the magnetic ground states of $CrSe_2$/$CrTe_2$ monolayers, which has also been found in other Cr-based systems [34–36].

To further investigate the origin of the magnetic evolution under applied strain, we plot in Fig. 6 the partial density of states (PDOS) of Cr $3d$ and Se $4p$ (Te $5p$) electrons for $CrSe_2$ ($CrTe_2$) monolayers at different tensile strains, at which the systems are in the FM states. It can be seen that the Cr $3d$ states are almost totally spin polarized and become the main contribution of the magnetism, so the magnetic moments of the Cr atoms are much larger than those of the Se/Te atoms, as shown in Fig. 4(c). The hybridization between Cr $3d$ and Se $4p$ (Te $5p$) orbitals is strong for the spin-up states, indicating the covalent character of the Cr-Se or Cr-Te bonds. For the $CrSe_2$ monolayer, both the Cr $3d$ and Se $4p$ orbitals become more localized near the Fermi level when the strain is increased [from Figs. 6(a)

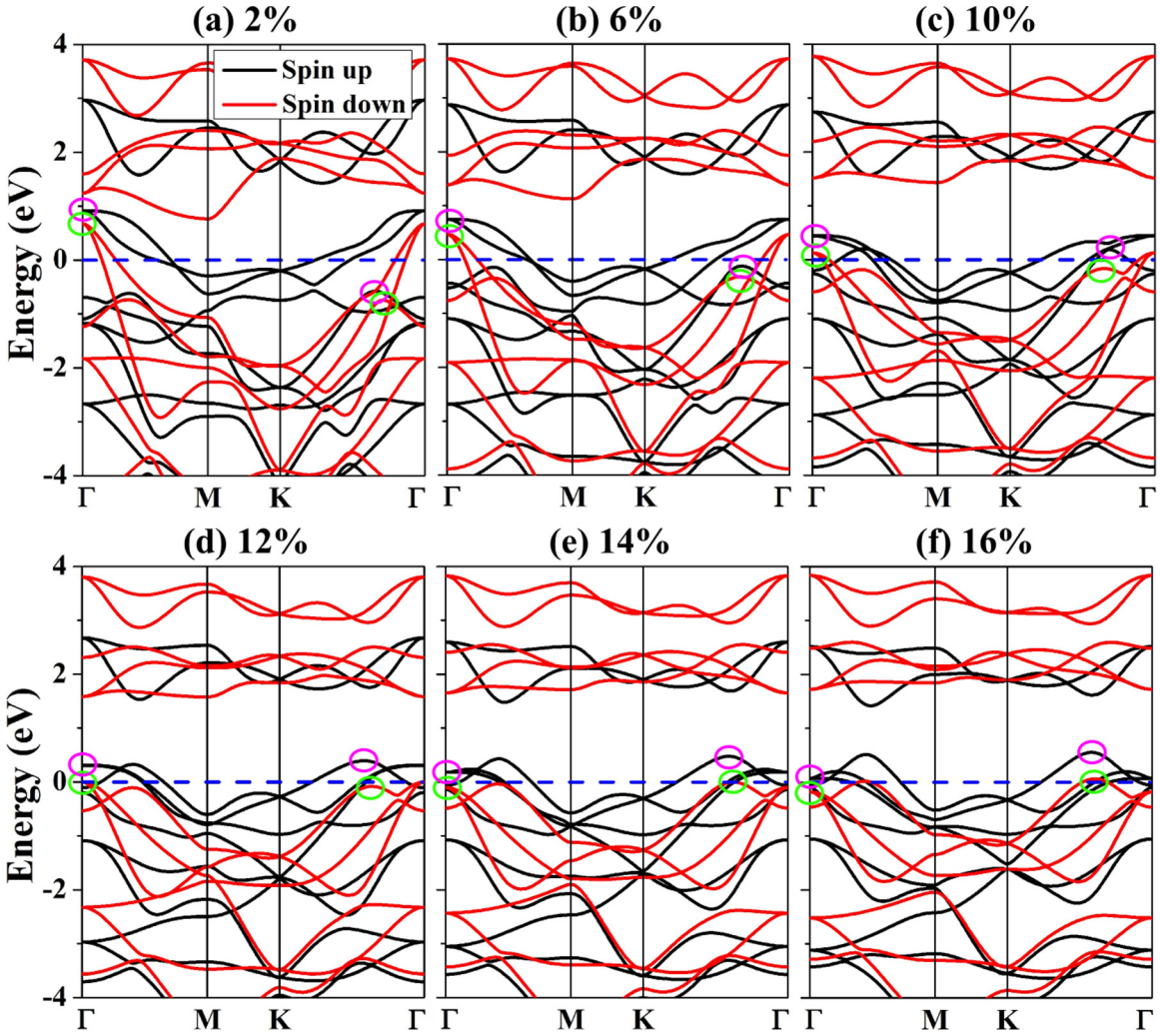

FIG. 7. (Color online) Band structures of the $CrSe_2$ monolayer in the FM ground states at tensile strains of (a) 2%, (b) 6%, (c) 10%, (d) 12%, (e) 14%, and (f) 16%. The Fermi level is set to be 0 eV.

to 6(c)]. At a strain of 10%, the peaks of the Cr $3d$ and Se $4p$ orbitals near the Fermi level appear at around -0.73 and 0.17 eV, respectively, and the hybridization of the two orbitals weakens, leading to more unpaired electrons near the Cr and Se atoms. The increasingly localized PDOS indicates a charge redistribution and increased magnetic moments on both Cr and Se atoms, as shown in Fig. 4(c). It is noted that at a strain of 10%, both the Cr $3d$ and Se $4p$ states become almost totally spin polarized and the $CrSe_2$ monolayer is nearly half metallic. We further increase the strain to 16% and find that in the strain range of 12%–16%, the system retains half metallic. For the $CrTe_2$ monolayer, however, the spin polarization of the Te $5p$ state becomes largest at a strain range of 4%–6% and weakens with a further increase of strain, which is consistent with the result that the magnetic moment of the Te atom is largest at this strain range. Since both the Cr $3d$ and Te $5p$ states cannot be totally spin polarized, the $CrTe_2$ monolayer remains metallic for the strain range investigated.

Two-dimensional half-metallic ferromagnets are highly desirable for future applications in high-performance spintronic devices. To see clearly how the half-metallic property takes place in the $CrSe_2$ monolayer, we plot in Fig. 7 band structures under different tensile strains, in which the system is in the FM ground state. For the spin-up energy band (drawn in black), the band extremum located at the Γ point (circled by the purple line) is gradually lowered as the strain is increased, while the band extremum along the K-Γ direction (also circled by the purple line) is elevated gradually. At a strain of 10%, when the first band extremum has not been lowered below the E_F, the second band extremum has already moved up above the E_F and keeps moving up with increasing strain, so the spin-up state remains metallic for the strain range investigated. For the spin-down energy band (drawn in red), however, the band extremum at the Γ point (circled by the green line) is lowered much faster than that of the spin-up state when strain is increased. At a strain of 12%, the band extremum at the Γ point moves below the E_F, with the band extremum along the K-Γ direction also residing below the E_F, so the spin-down state tends to be semiconducting with a sizable band gap of 1.58 eV. When the strain is further increased, the second extremum moves up very slowly and remains below the E_F, so the $CrSe_2$ monolayer remains half metallic in the strain range of 12%–16%.

IV. CONCLUSION

In conclusion, we have investigated the magnetic properties of $CrSe_2/CrTe_2$ monolayers under in-plane biaxial tensile and compressive strains. When no strain is applied, the $CrSe_2$ and $CrTe_2$ monolayers are found to be AFM and FM, respectively, consistent with their corresponding bulk counterparts. For the $CrSe_2$ monolayer, when the tensile strain reaches 2%, the system tends to be FM. Furthermore, the FM state is stabilized and the Curie temperature T_C as well as the magnetic moments increase with an increase in tensile strain. A relatively small strain of 4% can enhance the T_C to be 363.1 K, above room temperature. Moreover, the $CrSe_2$ monolayer changes from a metal to a half metal when the strain is larger than 10%. For the $CrTe_2$ monolayer, however, the critical strain at which the switch between FM and AFM states occurs is compressive, of -1%. When the tensile strain is larger than 2%, the T_C of the $CrTe_2$ monolayer can be higher than room temperature. The strain-tunable magnetic properties of the $CrSe_2$ ($CrTe_2$) monolayers can be understood by the competition between the AFM Cr-Cr direct exchange interaction and the FM Cr-Se(Te)-Cr superexchange interaction. Our results indicate that the strain is an effective way to tune the magnetic and electronic properties of $CrSe_2/CrTe_2$ monolayers.

In the experiments, strain can be applied to a 2D material in different ways. Traditionally, strain can arise from a lattice mismatch between substrates and epitaxial thin films [37]. In recent years, with the advances in nanotechnology, one can transfer a few-layer film to a soft polydimethylsiloxane (PDMS) substrate and strain can be applied to the film by either stretching [38,39] or bending [40,41] the supporting substrate. By using this method, strain as high as 30% has been realized in graphene [38,41]. Moreover, flexible graphene-based transistors have been successfully produced, which can operate in a large range of strains [42–44]. The reported methods of applying strain can be readily transferred to $CrSe_2/CrTe_2$ monolayers. The two monolayers are potential candidates for future nanoelectronic applications, which deserve further study in experiments.

ACKNOWLEDGMENTS

This work was supported by the National Key Basic Research under Contract No. 2011CBA00111, the National Natural Science Foundation of China under Contracts No. 11274311, No. 11404340, and No. U1232139, the Anhui Provincial Natural Science Foundation under Contract No. 1408085MA11, the China Postdoctoral Science Foundation (Grant No. 2014M550352), and the Special Financial Grant from the China Postdoctoral Science Foundation (Grant No. 2015T80670). The calculation was partially performed at the Center for Computational Science, CASHIPS.

[1] J. N. Coleman, M. Lotya, A. O'Neill, S. D. Bergin, P. J. King, U. Khan, K. Young, A. Gaucher, S. De, R. J. Smith, I. V. Shvets, S. K. Arora, G. Stanton, H.-Y. Kim, K. Lee, G. T. Kim, G. S. Duesberg, T. Hallam, J. J. Boland, J. J. Wang, J. F. Donegan, J. C. Grunlan, G. Moriarty, A. Shmeliov, R. J. Nicholls, J. M. Perkins, E. M. Grieveson, K. Theuwissen, D. W. McComb, P. D. Nellist, and V. Nicolosi, Science **331**, 568 (2011).

[2] R. J. Smith, P. J. King, M. Lotya, C. Wirtz, U. Khan, S. De, A. O'Neill, G. S. Duesberg, J. C. Grunlan, G. Moriarty, J. Chen, J. Wang, A. I. Minett, V. Nicolosi, and J. N. Coleman, Adv. Mater. **23**, 3944 (2011).

[3] S. Jeong, D. Yoo, M. Ahn, P. Miró, T. Heine, and J. Cheon, Nat. Commun. **6**, 5763 (2015).

[4] K. F. Mak, C. Lee, J. Hone, J. Shan, and T. F. Heinz, Phys. Rev. Lett. **105**, 136805 (2010).

[5] A. Splendiani, L. Sun, Y. Zhang, T. Li, J. Kim, C.-Y. Chim, G. Galli, and F. Wang, Nano Lett. **10**, 1271 (2010).

[6] T. Eknapakul, P. D. C. King, M. Asakawa, P. Buaphet, R.-H. He, S.-K. Mo, H. Takagi, K. M. Shen, F. Baumberger, T. Sasagawa, S. Jungthawan, and W. Meevasana, Nano Lett. **14**, 1312 (2014).

[7] Y. C. Cheng, Z. Y. Zhu, W. B. Mi, Z. B. Guo, and U. Schwingenschlögl, Phys. Rev. B **87**, 100401(R) (2013).

[8] A. Ramasubramaniam and D. Naveh, Phys. Rev. B **87**, 195201 (2013).

[9] R. Mishra, W. Zhou, S. J. Pennycook, S. T. Pantelides, and J.-C. Idrobo, Phys. Rev. B **88**, 144409 (2013).

[10] C. J. Gil, A. Pham, A. Yu, and S. Li, J. Phys.: Condens. Matter **26**, 306004 (2014).

[11] H. Shi, H. Pan, Y.-W. Zhang, and B. I. Yakobson, Phys. Rev. B **88**, 205305 (2013).

[12] H. Pan, J. Phys. Chem. C **118**, 13248 (2014).

[13] H. Pan, Sci. Rep. **4**, 7524 (2014).

[14] P. Manchanda, V. Sharma, H. Yu, D. J. Sellmyer, and R. Skomski, Appl. Phys. Lett. **107**, 032402 (2015).

[15] H. Zhang, X.-B. Li, and L.-M. Liu, J. Appl. Phys. **114**, 093710 (2013).

[16] X. Mao, Y. Xu, Q. Xue, W. Wang, and D. Gao, Nanoscale Res. Lett. **8**, 430 (2013).

[17] Y. Ma, Y. Dai, M. Guo, C. Niu, Y. Zhu, and B. Huang, ACS Nano **6**, 1695 (2012).

[18] Y. Zhou, Z. Wang, P. Yang, X. Zu, L. Yang, X. Sun, and F. Gao, ACS Nano **6**, 9727 (2012).

[19] M. Kan, S. Adhikari, and Q. Sun, Phys. Chem. Chem. Phys. **16**, 4990 (2014).

[20] D. C. Freitas, R. Weht, A. Sulpice, G. Remenyi, P. Strobel, F. Gay, J. Marcus, and M. Núñez-Regueiro, J. Phys.: Condens. Matter **27**, 176002 (2015).

[21] D. C. Freitas, M. Núñez, P. Strobel, A. Sulpice, R. Weht, A. A. Aligia, and M. Núñez-Regueiro, Phys. Rev. B **87**, 014420 (2013).

[22] P. Hohenberg and W. Kohn, Phys. Rev. **136**, B864 (1964).

[23] P. Giannozzi, S. Baroni, N. Bonini, M. Calandra, R. Car, C. Cavazzoni, D. Ceresoli, G. L. Chiarotti, M. Cococcioni, I. Dabo, A. Dal Corso, S. de Gironcoli, S. Fabris, G. Fratesi, R. Gebauer, U. Gerstmann, C. Gougoussis, A. Kokalj, M. Lazzeri, L. Martin-Samos, N. Marzari, F. Mauri, R. Mazzarello,

S. Paolini, A. Pasquarello, L. Paulatto, C. Sbraccia, S. Scandolo, G. Sclauzero, A. P. Seitsonen, A. Smogunov, P. Umari, and R. M. Wentzcovitch, J. Phys.: Condens. Matter **21**, 395502 (2009).
[24] J. P. Perdew, K. Burke, and M. Ernzerhof, Phys. Rev. Lett. **77**, 3865 (1996).
[25] R. W. Williams, T. L. Loucks, and A. R. Mackintosh, Phys. Rev. Lett. **16**, 168 (1966).
[26] C. Kittel, in *Solid State Physics*, edited by F. Seitz, D. Turnbull, and H. Ehrensch (Academic, New York, 1968), Vol. 22, p. 1.
[27] S. Legvold, in *Ferromagnetic Materials*, edited by E. P. Wohlfhart (North-Holland, Amsterdam, 1980), Vol. 1, p. 191.
[28] M. Biasini, G. Ferro, G. Kontrym-Sznajd, and A. Czopnik, Phys. Rev. B **66**, 075126 (2002).
[29] B. van Laar and D. J. W. Ijdo, J. Solid State Chem. **3**, 590 (1971).
[30] J. Kudrnovský, I. Turek, V. Drchal, F. Máca, P. Weinberger, and P. Bruno, Phys. Rev. B **69**, 115208 (2004).
[31] J. B. Goodenough, Phys. Rev. **100**, 564 (1955).
[32] J. Kanamori, J. Appl. Phys. **31**, S14 (1960).
[33] P. W. Anderson, Phys. Rev. **115**, 2 (1959).
[34] C. M. Fang, P. R. Tolsma, C. F. van Bruggen, R. A. de Groot, G. A. Wiegers, and C. Haas, J. Phys.: Condens. Matter **8**, 4381 (1996).
[35] C. M. Fang, C. F. van Bruggen, R. A. de Groot, G. A. Wiegers, and C. Haas, J. Phys.: Condens. Matter **9**, 10173 (1997).
[36] X. F. Chen, J. S. Qi, and D. N. Shi, Phys. Lett. A **379**, 60 (2015).
[37] G. Gao, S. Jin, and W. Wu, Appl. Phys. Lett. **90**, 012509 (2007).
[38] K. S. Kim, Y. Zhao, H. Jang, S. Y. Lee, J. M. Kim, K. S. Kim, J.-H. Ahn, P. Kim, J.-Y. Choi, and B. H. Hong, Nature (London) **457**, 706 (2009).
[39] M. A. Bissett, S. Konabe, S. Okada, M. Tsuji, and H. Ago, ACS Nano **7**, 10335 (2013).
[40] S.-I. Park, J.-H. Ahn, X. Feng, S. Wang, Y. Huang, and J. A. Rogers, Adv. Funct. Mater. **18**, 2673 (2008).
[41] Y. Wang, R. Yang, Z. Shi, L. Zhang, D. Shi, E. Wang, and G. Zhang, ACS Nano **5**, 3645 (2011).
[42] B. J. Kim, H. Jang, S.-K. Lee, B. H. Hong, J.-H. Ahn, and J. H. Cho, Nano Lett. **10**, 3464 (2010).
[43] S.-K. Lee, B. J. Kim, H. Jang, S. C. Yoon, C. Lee, B. H. Hong, J. A. Rogers, J. H. Cho, and J.-H. Ahn, Nano Lett. **11**, 4642 (2011).
[44] C.-C. Lu, Y.-C. Lin, C.-H. Yeh, J.-C. Huang, and P.-W. Chiu, ACS Nano **6**, 4469 (2012).